

A&A manuscript no.
(will be inserted by hand later)

Your thesaurus codes are:
08 (08.14.1; 08.19.4; 02.04.1; 02.05.2)

ASTRONOMY
AND
ASTROPHYSICS
5.10.2018

Influence of the symmetry energy on the birth of neutron stars and supernova neutrinos

K. Sumiyoshi¹, H. Suzuki², and H. Toki^{1,3}

¹ The Institute of Physical and Chemical Research (RIKEN),
Hirosawa, Wako, Saitama 351-01, Japan
e-mail: sumi@postman.riken.go.jp

² National Laboratory for High Energy Physics (KEK),
Oho, Tsukuba, Ibaraki 305, Japan
e-mail: suzuki@kekth1.kek.jp

³ Research Center for Nuclear Physics (RCNP), Osaka University
Mihogaoka, Ibaraki, Osaka 567, Japan
e-mail: toki@rcnpvx.rcnp.osaka-u.ac.jp

Received February 2, 1995; accepted March 27, 1995

Abstract. We study the influence of the symmetry energy of the equation of state on the thermal evolution of protoneutron stars and the properties of supernova neutrinos by the numerical simulations after the protoneutron stars are formed. As for the equation of state (EOS) of nuclear matter, we take two EOS's with different symmetry energies obtained by the relativistic mean field theory. We find the symmetry energy plays the essential role on the evolution of lepton profiles and the neutrino fluxes.

Key words: stars: neutron – supernovae: general – dense matter – equation of state

influence of the symmetry energy on astrophysical problems.

The effects of the symmetry energy on the evolution of neutron stars and supernovae have been studied by several authors. The possibility of the rapid cooling of neutron stars due to the direct URCA process has been discussed in the case of the large proton fraction of neutron star matter, which is sensitive to the density dependence of the symmetry energy (Boguta 1981; Lattimer et al. 1991). Bruenn (1989) studied the effects on supernova explosions systematically by doing numerical simulations of gravitational core collapse with the parameterized EOS. Swesty et al. (1994) also studied the role in the prompt phase of the supernova explosion. However, there has been no systematic study on the effect of the symmetry energy on the birth of neutron stars and supernova neutrinos as far as we know. Moreover, in most of previous studies, the parameterized formula have been used to provide the EOS of dense matter beyond the normal nuclear matter density.

Recently, there has been a great progress in the study of nuclei and dense matter within the relativistic many body framework (Serot & Walecka 1986). It was demonstrated that the relativistic Brueckner Hartree Fock (RBHF) theory is capable of reproducing the saturation property of nuclear matter starting from the nucleon-nucleon interaction determined by the scattering experiments (Brockmann & Machleidt 1990). The relativistic mean field (RMF) theory has been shown to be very successful as an effective theory to describe the ground state properties of nuclei in the wide mass range of the periodic

1. Introduction

The recent advance in radioactive nuclear beam experiments provides us with novel information on unstable nuclei far away from the stability line (Tanihata et al. 1985). The symmetry energy becomes more essential to understand the nuclear structure as we go further away from stability. The symmetry energy is also important to provide the equation of state (EOS) for neutron stars and supernovae. The properties of dense matter under neutron rich environment determine the structure and chemical composition of stars and may change their evolution drastically. Therefore, it is very interesting to study the

Send offprint requests to: K. Sumiyoshi

table (Gambhir et al. 1990) and has been applied to the EOS for neutron stars (Serot & Walecka 1986). It is amazing that the RMF theory describes also the properties of unstable nuclei away from stability extremely well (Hirata et al. 1991; Sugahara & Toki 1994). Having the framework constrained by unstable nuclei, Sumiyoshi and Toki applied the same RMF theory to provide the data table of the EOS for neutron stars and supernovae (Sumiyoshi & Toki 1994; Sumiyoshi et al. 1995), which enables us to do numerical simulations of the thermal evolution of neutron stars and supernovae quantitatively while taking care of the experimental data of unstable nuclei. The properties of unstable nuclei have been shown to be very sensitive to the symmetry energy in the RMF theory (Sumiyoshi et al. 1993a). Hence, it would be nice if we could see how sensitive are the properties of neutron stars to the symmetry energy and what is the influence of the symmetry energy on the birth of neutron stars and supernova neutrinos.

The numerical simulations of the cooling of protoneutron stars and neutrino burst have been done by several groups (Burrows & Lattimer 1986; Burrows 1988; Suzuki 1993). The influence on the numerical simulation of the birth of neutron stars due to the difference of EOS was studied by adopting the EOS tables in the two different many body frameworks (Sumiyoshi et al. 1993b). The effects of various thermodynamical properties were pointed out there besides the stiffness of EOS, which has been mainly studied so far (Burrows 1988). Here, we focus on the influence of the symmetry energy by changing solely the strength of the isovector interaction in the RMF theory in order to see its effect clearly.

The purpose of this paper is to explore the influence of the symmetry energy on the cooling of protoneutron stars just born in supernova explosions. We construct the tables of EOS for supernova simulations in the RMF theory and make comparisons of EOS's when we change the symmetry energy drastically. Then, we perform numerical simulations of the birth of neutron stars and supernova neutrinos adopting the two EOS's with different symmetry energy. We investigate the influence of the symmetry energy on the thermal evolution of protoneutron stars and the properties of neutrino burst emitted during the cooling stage.

This paper is arranged as follows. In section 2, we briefly describe the relativistic EOS for neutron stars and supernovae. In section 3, after a short introduction on the birth of neutron stars, we present the results of our numerical simulations. We discuss the effects of the symmetry energy on the deleptonization, the thermal evolution and the supernova neutrinos in the subsections. We summarize this paper in section 4.

2. Relativistic equation of state

We start with a brief explanation of the tables of EOS for numerical simulations. We calculate all the physical quan-

ties of dense matter within the relativistic mean field theory. We refer the review article by Serot & Walecka (1986) as for the relativistic many body framework for nuclei and dense matter. All the details on the relativistic EOS for neutron stars and supernovae in the RMF theory has been reported in the recent papers. (Sumiyoshi & Toki 1994; Sumiyoshi et al. 1995).

We adopt the phenomenological lagrangian with the non-linear σ and ω terms, which is motivated by the recent success of the RBHF theory (Brockmann & Machleidt 1990) and has been shown to be very successful both for nuclear properties and dense matter (Sugahara & Toki 1994). The best parameter set for the lagrangian, named TM1, was determined by the least square fitting to a set of nuclei including unstable ones, which is important to constrain the isovector interaction in the theory. It is remarkable that the RMF theory with the parameter set TM1 has been demonstrated to reproduce successfully the properties of unstable nuclei other than the ones used in the fitting. The properties of nuclear matter in the RMF theory with TM1 thus constrained has been shown to be quite similar to the properties of nuclear matter derived in the RBHF theory (Sugahara & Toki 1994). Extending the RMF theory to the case at finite temperature, the table of the numerical data of physical quantities under various conditions of chemical composition, temperature and density, which are required for the numerical simulations, was constructed for the parameter set TM1 (Sumiyoshi et al. 1995). We use this table of EOS as a standard one.

In order to explore the influence of the symmetry energy, we newly construct the table of EOS with a reduced value of the symmetry energy in the RMF theory. We reduce the value of the coupling constant g_ρ between isovector-vector ρ meson and nucleon in the lagrangian, which is essential to determine the symmetry energy, while keeping other parameters of TM1 unchanged. Hereafter, we call the modified parameter set as TMS. The symmetry energy is $a_{sym} = 36.9$ MeV for TM1 and $a_{sym} = 28.2$ MeV for TMS: the corresponding coupling constant is $g_\rho = 4.63$ for TM1 and $g_\rho = 3.50$ for TMS. We note that the symmetry energy in TM1 has been checked by unstable nuclei and this modification in TMS is to explore the effect of the symmetry energy on astrophysical applications. We display in Fig. 1 the energy per baryon of symmetric nuclear matter and pure neutron matter for the cases of TM1 and TMS. The incompressibility K at the normal nuclear matter density is 281 MeV for both cases, since the isovector meson does not contribute to symmetric nuclear matter.

We comment here on the density dependence of the symmetry energy. The symmetry energy for both cases of TM1 and TMS has a monotonically increasing feature with density, which is common for all the relativistic many body calculations due to the contribution of the isovector meson. This feature is demonstrated by the microscopic calculation with the use of the RBHF theory (Li et al. 1992). The reduction of the symmetry energy at the sat-

uration density by changing the strength of the isovector interaction clearly corresponds to the reduction of the symmetry energy at high density. In contrast, the symmetry energy in the non-relativistic many body calculations such as the one by Wiringa et al. (1988) has generally a weak density dependence and has sometimes a decreasing feature at high density. A variety of the density dependence depends on the choice of the density dependent potential, which is introduced to reproduce the saturation of nuclear matter. Therefore, the relation between the symmetry energy at the saturation density and its behavior at high density is ambiguous in non-relativistic many body calculations.

When we apply the EOS's in the two cases to neutron stars, we found that the chemical compositions are very different while the hydrostatic structures are quite similar. In Fig. 2-a, we display the proton fraction of neutron star matter, which is the ratio between the proton density and the baryon density, as a function of the baryon mass density. The proton fraction in the case of TMS is smaller than the case of TM1 because of the reduced symmetry energy. We show in Fig. 2-b the neutron star mass as a function of the central baryon mass density. In contrast to the difference in the chemical composition, the neutron star masses in the two cases are found very similar. The maximum mass turns out to be almost the same value of $2.2 M_{\odot}$. The difference in the central baryon mass density is only about 1% for the case of neutron stars with the gravitational mass of $1.4 M_{\odot}$.

3. Evolution of protoneutron stars

First of all, we describe briefly the supernova explosions and the birth of neutron stars (Suzuki 1994). Gravitational collapse of the core of a massive star leads to explosion of the envelope (supernova explosion) and formation of the neutron star. We shall divide the series of stages starting from the onset of the core collapse to the birth of neutron star into two phases.

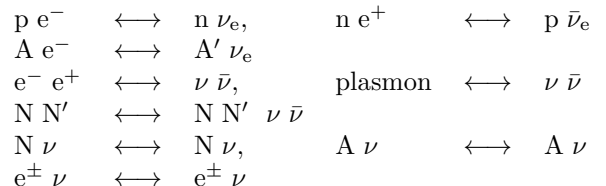
The first phase is the dynamical phase. The core of a massive star becomes unstable when it grows to the point near the Chandrasekhar mass ($\sim 1.4 M_{\odot}$), and it begins to collapse. The collapse never ceases until the central density exceeds the nuclear density. Sudden stiffening of the EOS above the nuclear density stops the inner core ($0.5 - 0.8 M_{\odot}$) and the bounce of the inner core launches a shock wave into the falling outer core. The matter of the falling outer core is swept and decelerated by the shock wave and, then, accretes onto the unshocked inner core which has been in hydrostatic equilibrium in its dynamical time scale of milliseconds. The shock wave expels the envelope and we identify it as supernova explosion. The remnant at the center which consists of the unshocked inner core and the shocked outer core is called as a protoneutron star. It contains so many leptons and protons ($\sim 30\%$) that we

cannot call it a neutron star at this stage. It takes only about 1 second for this dynamical process to take place.

The second phase, which is the quasistatic phase of protoneutron star cooling, follows this dynamical phase. After the shock wave breaks out of the core surface and the accretion onto the inner core ceases, the protoneutron star evolves quasistatically keeping hydrostatic configuration. Neutrinos which are trapped in the core diffuse out of the protoneutron star in a time scale of neutrino diffusion, which is of order of 10 seconds. They drive the evolution of the protoneutron star into the cold neutron star by carrying out thermal energy and lepton number from the protoneutron star. Concerning supernova neutrinos, about a half of the total energy is emitted during the dynamical phase and the rest is emitted during the quasistatic phase.

In this paper, we study the influence of the nuclear symmetry energy on the second stage: the evolution of the hot protoneutron star into the normal neutron star. The quasistatic cooling of the protoneutron star is simulated numerically by solving the general relativistic equations for hydrostatic structure (Oppenheimer-Volkoff equation) and for neutrino transport with the deleptonization and the entropy change of the matter simultaneously using the Henyey-type method. As for the neutrino transfer, we adopt the multigroup flux limited diffusion scheme (Bruenn 1985). We take into account the energy dependence of neutrino transport coefficients in the multigroup scheme. The flux limiter should be introduced in order to express the neutrino flux in the transparent regime in terms of the diffusion flux. We adopt Mayle and Wilson's flux limiter (Mayle et al. 1987) in this work. We include the general relativistic effects such as the time dilation and the red shift of the neutrino energy. We treat explicitly, ν_e , $\bar{\nu}_e$ and $\nu_{\mu/\tau}$, where $\nu_{\mu/\tau}$ represents the average of ν_{μ} , $\bar{\nu}_{\mu}$, ν_{τ} and $\bar{\nu}_{\tau}$. This is a good approximation in the case where we can neglect the existence of μ and τ leptons because of the low temperature ($\lesssim 100$ MeV).

The following neutrino interactions are included as opacity sources or collision terms in the neutrino transfer equations.



where ν represents all species of neutrinos, A is a representative heavy nucleus, and N is either a proton or a neutron. Most of the interaction rates are taken from Bruenn (1985) with some modifications. At present, many body effects on neutrino opacity are not included except for the multiple scattering suppression effects on nucleon bremsstrahlung process (Raffelt & Seckel 1991). The evolution of the protoneutron star is driven by the exchange of energy and lepton number between the matter and neutrinos due to

the above interactions and the neutrino transport. Descriptions of our numerical code are also given in Suzuki (1993).

We perform numerical simulations of the protoneutron star evolution using the tables of EOS in the RMF theory with TM1 and TMS. As for the EOS of the low density matter ($\rho \leq 10^{14} \text{g/cm}^3$), Wolff's EOS (Hillebrandt & Wolff 1985) is used for both cases. We construct the initial models for our numerical simulation by referring to the numerical results of Mayle and Wilson at 0.4 sec after the core bounce in the hydrodynamical simulations of the supernova explosion (Mayle & Wilson 1989; Wilson 1990). Initial models for the simulations using the two EOS's are constructed using the same entropy profile and the same electron fraction profile in order to study the effects of the difference in the symmetry energy. Of course, in principle, these profiles should differ from each other because the difference of EOS should also affect on the dynamical phase. To extract the direct influence of the nuclear symmetry energy on the protoneutron star evolution, we neglect its influence on the dynamical phase.

The calculated initial hydrostatic structures of the two protoneutron stars are found similar; the differences in the initial densities and the temperature profiles are smaller than 3%. On the contrary, there is a large difference in $\mu_\nu^{eq} \equiv \mu_p + \mu_e - \mu_n$ which is the chemical potential of ν_e in the β -equilibrium with the matter because μ_p and μ_n are directly affected by the symmetry energy. In Figs. 3–8, we present the profiles of the two initial models. μ_ν^{eq} at the center of the initial models are 142 MeV ($a_{sym} = 36.9 \text{ MeV}$) for TM1 and 170 MeV for TMS ($a_{sym} = 28.2 \text{ MeV}$), respectively. The resultant lepton fractions, $Y_L = (n_{e^-} + n_{\nu_e} - n_{e^+} - n_{\bar{\nu}_e})/n_{\text{baryon}}$ are 0.330 for TMS and 0.315 for TM1.

3.1. Deleptonization

Starting from these initial models we simulate the evolution of the protoneutron stars for the following 15 seconds with the same numerical code. Figs. 3–8 also show the profiles of the protoneutron stars at the end of the calculation ($t = 15 \text{ sec}$) for the two models. While the density profiles are still nearly identical, the distributions of the temperature and the electron fraction differ largely from each other. Especially, the lepton fraction at the center for TM1 (0.179) is larger than that for TMS (0.155), while the former is smaller than the latter at the initial stage. This means that the deleptonization proceeds faster for TMS than for TM1. We find that this is caused by the difference of μ_ν^{eq} . In the central region of protoneutron stars, electron type neutrinos are degenerate and their diffusion fluxes are roughly proportional to $-\lambda_\nu \partial n_{\nu_e} / \partial r$, where λ_ν is the mean free path of ν_e and n_{ν_e} is the number density of ν_e . λ_ν is roughly inversely proportional to the neutrino energy squared, $\lambda_\nu \propto (\mu_\nu^{eq})^{-2}$, and $n_{\nu_e} \propto (\mu_\nu^{eq})^3$ in the degenerate limit. Consequently, the diffusion flux in the

degenerate limit is proportional to $-\partial \mu_\nu^{eq} / \partial r$; the smaller symmetry energy results in the larger μ_ν^{eq} , the larger ν_e flux, and therefore the faster deleptonization.

3.2. Thermal evolution

The influence of the symmetry energy on the evolution of the temperature is complicated in our models. The central temperature at $t = 15 \text{ sec}$ are 23.2 MeV for TM1 and 26.3 MeV for TMS. Higher temperature for TMS is due to the higher total (matter + neutrinos) entropy per baryon (1.29 for TMS and 1.20 for TM1) and the lower lepton fraction (0.155 for TMS and 0.179 for TM1). The lower lepton fraction which is the consequence of fast deleptonization means the smaller lepton number density and the temperature corresponding to a given total entropy becomes higher.

As for the difference in the central entropy, we analyze the results of numerical simulations in detail and find the following reason for the present case. In the first 10 seconds of the protoneutron star cooling, the matter entropy of the central region increases. This entropy change has three main origins; inward flux of $\nu_{\mu/\tau}$, the downscattering of ν_e and the emission of ν_e due to electron capture. Since, during the first 10 seconds, the temperature profile has its peak in the middle region of the protoneutron star, not at the center, there is the negative gradient in the number density of $\nu_{\mu/\tau}$ at the central region. The flux of $\nu_{\mu/\tau}$ is proportional to the gradient. Therefore, at the early stage, $\nu_{\mu/\tau}$ flow inwards in the central region and transport the heat into the central region from the middle region. The pair annihilations of $\nu_{\mu/\tau}$ ($\nu_\mu \bar{\nu}_\mu / \nu_\tau \bar{\nu}_\tau \rightarrow e^- e^+$) increase the matter entropy. In addition, in the central region where the electrons are strongly degenerate, ν_e -electron scattering ($\nu_e e^- \rightarrow \nu_e e^-$) leads to the increase of the matter entropy. Neutrinos lose their energy at the scattering (downscattering) because the scattered electrons which were within the Fermi sea should have energy greater than the Fermi energy. On the other hand, emission of ν_e ($pe^- \rightarrow \nu_e n$) decreases the matter entropy. The two heating processes and the one cooling process result in the net heating of the central region.

Detailed analysis of the numerical simulations reveals that, among the above three processes which alter the central entropy, the largest difference of heating/cooling rate ($dS_{mat}/dt(r=0)$) due to each process between the two models is the difference of the cooling rate due to the ν_e emission. Furthermore it is found that the difference in $dS_{mat}/dt(r=0)$ due to the ν_e emission is caused mainly by the difference of μ_ν^{eq} as the case of the deleptonization rate. dS_{mat}/dt due to $pe^- \leftrightarrow \nu_e n$ can be expressed as

$$\begin{aligned} & \left. \frac{dS_{mat}}{dt} \right|_{pe^- \leftrightarrow \nu_e n} \\ &= -\frac{1}{T n_{\text{baryon}}} \left(\left. \frac{\partial u_{\nu_e}}{\partial t} \right|_{pe^- \leftrightarrow \nu_e n} - \mu_\nu^{eq} \left. \frac{\partial n_{\nu_e}}{\partial t} \right|_{pe^- \leftrightarrow \nu_e n} \right) \quad (1) \end{aligned}$$

where u_{ν_e} is the energy density of ν_e . Since, in the central region at the early stage where the electron capture proceeds, $\partial n_{\nu_e}/\partial t|_{\text{pe}^- \leftrightarrow \nu_e \text{n}}$ is positive, it can be seen that the larger μ_{ν}^{eq} for the smaller symmetry energy results in the larger dS_{mat}/dt due to ν_e emission, that is, the less entropy loss of the matter because $dS_{\text{mat}}/dt|_{\text{pe}^- \leftrightarrow \nu_e \text{n}}$ is negative there. This small cooling rate due to the ν_e emission leads to the higher entropy and higher temperature for the case of smaller symmetry energy. We note, however, that the temperature profile is affected by many factors.

3.3. Supernova neutrinos

The difference in the evolutions of the protoneutron star due to the symmetry energy is reflected with the properties of supernova neutrinos emitted during the cooling stage of the star. We show in Fig. 9 the net flux of the electron type lepton number from the protoneutron star; the flux of ν_e minus $\bar{\nu}_e$. The net flux is larger for TMS than for TM1 during 15 seconds because of the difference in the diffusion fluxes as we have discussed in section 3.1. This fact corresponds to the higher deleptonization rate in TMS having the smaller symmetry energy. Since the final electron fraction of the neutron star at the end of the deleptonization is smaller for TMS, the total net neutrino number emitted during the cooling is larger for TMS than for TM1. It may be possible to extract the information of the final electron fraction of the neutron star from this quantity.

We show in Fig. 10 the calculated time profile of the mean energy of $\bar{\nu}_e$. The mean energy for TMS becomes higher than that for TM1 at a later stage. This is due to the difference of the temperature profile of the protoneutron stars, as shown in Fig. 4. The mean energy of neutrinos depends mainly on the temperature at the neutrinosphere. The difference of the mean energies is larger for $\nu_{\mu/\tau}$ and smaller for ν_e depending on the position of its neutrinosphere. The neutrinosphere for ν_e which interact most strongly with the matter locates in the outermost region, where both the temperature and the density are low and the difference between the temperature in the two cases is small.

We show in Fig. 11 the luminosity of $\bar{\nu}_e$, which is higher for TMS than for TM1. The general feature is quite similar for the other types of neutrinos. These results correspond to the larger flux and the higher mean energy of neutrinos. The total energy carried out by neutrinos is larger for TMS than for TM1, since the gravitational mass of the neutron star at zero temperature is smaller for TMS. We note that the total baryon mass of the protoneutron stars is fixed to be $1.62 M_{\odot}$ (the gravitational mass of the initial protoneutron star is $1.5479 M_{\odot}$ for TMS and $1.5482 M_{\odot}$ for TM1) in the present study and the gravitational mass of the cold neutron star turns out to be $1.475 M_{\odot}$ for TMS and $1.485 M_{\odot}$ for TM1. Therefore, the total energy released from the protoneutron star amounts to $0.073 M_{\odot}$

($1.31 \cdot 10^{53}$ erg) for TMS and $0.063 M_{\odot}$ ($1.13 \cdot 10^{53}$ erg) for TM1, which means the larger luminosity for TMS, provided that the time duration of neutrino emission is similar.

4. Summary and Discussions

The main influence of the symmetry energy of the EOS on the birth of neutron stars comes from the change of the chemical composition rather than the stiffness. A change in the chemical potential for neutrinos affects the rates of the interaction with the matter even if the matter density is unchanged. It affects the deleptonization rate through the change of the diffusion flux, and the temperature inside stars through the change of the heating rate. Those changes influence the properties of the neutrino burst such as the time profile of the mean energy while the density profile remains unchanged. The difference in the properties of the neutrino burst is emphasized moreover by the difference in the proton fraction and the binding energy of the cold neutron stars at the end of the birth stage.

The above results come from our study on the evolution of protoneutron stars by assuming the same initial conditions following the result of Mayle & Wilson. Here we comment on expected difference in the initial protoneutron star configuration when we simulate also the dynamical phase, the birth of the protoneutron stars, using the two EOS's. Since TMS has a smaller coupling constant g_{ρ} , it is expected that the symmetry energy and hence the difference between the chemical potential of neutrons and that of protons are smaller for TMS than for TM1 even at the density of the collapsing core. This means a larger fraction of free protons for TMS, which will result in a larger electron-capture rate during the collapse and a smaller trapped lepton fraction at the core bounce (Bruenn 1989). Throughout the birth stage of neutron stars including both the dynamical phase and the quasistatic phase, deleptonization will proceed faster for TMS than for TM1 and electron-type lepton number flux will be larger for TMS. The work in this direction to simulate also the dynamical phase is in progress.

Further studies are required to predict precisely the profile of the neutrino burst and to extract the information on the symmetry energy from the observational signals of the next supernova explosion in our Galaxy or close-by. The influence of the thermodynamical properties of EOS such as the symmetry energy should be carefully examined besides the one by the stiffness, which has been mainly focused. The symmetry energy is one of the most interesting keys to clarify the current problems in nuclear physics and astrophysics. It would be interesting to apply the many body framework such as the RMF theory, in which the symmetry energy is being checked by the properties of unstable nuclei, to solve consistently the current issues on the cooling of the neutron stars and the supernova explosion together with the ones in nuclear physics.

Acknowledgements. We would like to thank K. Oyamatsu, S. Nishizaki, T. Takatsuka and K. Sato for comments and discussions, and R. Mayle, J. R. Wilson and R. G. Wolff for providing us with their data. We are grateful to Y. Sugahara, D. Hirata and I. Tanihata for providing us with valuable information and for fruitful discussions on the aspect of unstable nuclei. K. S. acknowledges the support by the Special Researchers' Basic Science Program.

References

- Boguta J., 1981, Phys. Lett. B106, 255
 Brockmann R., Machleidt R., 1990, Phys. Rev. C42, 1965
 Bruenn S. W., 1985, ApJS 58, 771
 Bruenn S. W., 1989, ApJ 340, 955
 Burrows A., Lattimer J. M., 1986, ApJ 307, 178
 Burrows A., 1988, ApJ 334, 891
 Gambhir Y. K., Ring P., Thimet A., 1990, Ann. of Phys. 198, 132
 Hillebrandt W., Wolff R. G., 1985, In: Arnett W. D., Truran J. W., (eds.) Nucleosynthesis: Challenges and New Developments, The University of Chicago Press, Chicago, p.131
 Hirata D., Toki H., Watabe T., Tanihata I., Carlson B. V., 1991, Phys. Rev. C44, 1467
 Lattimer J. M., Pethick C. J., Prakash M., Haensel P., 1991, Phys. Rev. Lett. 66, 2701
 Li G. Q., Machleidt R., Brockmann R., 1992, Phys. Rev. C45, 2782
 Mayle R., Wilson J. R., 1989, private communication
 Mayle R., Wilson J. R., Schramm D. N., 1987, ApJ 318, 288
 Raffelt G., Seckel D., 1991, Phys. Rev. Lett. 67, 2605
 Serot B. D., Walecka J. D., 1986, Adv. Nucl. Phys. 16, 1
 Sugahara Y., Toki H., 1994, Nucl. Phys. A579, 557
 Sumiyoshi K., Hirata D., Toki H., Sagawa H., 1993a, Nucl. Phys. A552, 437
 Sumiyoshi K., Suzuki H., Toki H., 1993b, In: Morrissey D. J. (ed.) Proceedings of the third International Conference on Radioactive Nuclear Beams, Michigan, USA, 1993, Editions Frontieres, Gif-sur-Yvette, p.501
 Sumiyoshi K., Toki H., 1994, ApJ 422, 700
 Sumiyoshi K., Kuwabara H., Toki H., 1995, Nucl. Phys. A581, 725
 Suzuki H., 1993, In: Suzuki Y., Nakamura K. (eds.) Proceedings of the International Symposium on Frontiers of Neutrino Astrophysics, Takayama, Japan, 1992, Universal Academy Press Inc., Tokyo, p.219
 Suzuki H., 1994, In: Fukugita M., Suzuki A. (eds.) Physics and Astrophysics of Neutrinos, Springer-Verlag, Tokyo, p.763, and references therein
 Swesty F. D., Lattimer J. M., Myra E. S., 1994, ApJ 425, 195
 Tanihata I., Hamagaki H., Hashimoto O., et al., 1985, Phys. Rev. Lett. 55, 2676
 Wilson J., 1990, Nucl. Phys. B.(Proc. Suppl.) 13, 380
 Wiringa R. B., Fiks V., Fabrocini A., 1988, Phys. Rev. C38, 1010

Figure Captions

Fig. 1. The energy per baryon of nuclear matter in the RMF theory is shown as a function of the baryon density for the cases with TM1 and TMS. The solid curves represent the results of symmetric nuclear matter and pure neutron matter with TM1. The dashed curve represents the result of pure neutron matter with TMS. The result of symmetric nuclear matter with TMS is the same as the one with TM1.

Fig. 2. a The proton fraction of neutron star matter is shown by the solid curve for the case with TM1 as a function of the baryon mass density. The dashed curve represents the case with TMS. **b** The gravitational masses of neutron stars with the EOS of neutron star matter in the RMF theory with TM1 (solid) and TMS (dashed) as functions of the central baryon mass density.

Fig. 3. The radial profiles of the matter entropy (S) at $t = 0$ sec (initial models) and at $t = 15$ sec. Solid lines are the model with TM1 and dashed lines are the model with TMS. The abscissa is the enclosed baryon mass (M_B) in units of the solar mass (M_\odot).

Fig. 4. The radial profiles of the temperature (T) at $t = 0$ sec (initial models) and at $t = 15$ sec in the same notation as Fig. 3.

Fig. 5. The radial profiles of the density (ρ_B) at $t = 0$ sec (initial models) and at $t = 15$ sec in the same notation as Fig. 3. The differences in density profiles between the two models are very small.

Fig. 6. The radial profiles of the electron fraction (Y_e) at $t = 0$ sec (initial models) and at $t = 15$ sec in the same notation as Fig. 3.

Fig. 7. The radial profiles of the lepton fraction (Y_L) at $t = 0$ sec (initial models) and at $t = 15$ sec in the same notation as Fig. 3.

Fig. 8. The radial profiles of the chemical potential of ν_e in β -equilibrium (μ_ν) at $t = 0$ sec (initial models) and at $t = 15$ sec in the same notation as Fig. 3.

Fig. 9. The time profiles of the net flux of the electron type lepton number are shown for the cases with TM1 and TMS by the solid curve and the dashed curve, respectively.

Fig. 10. The time profiles of the mean energy of $\bar{\nu}_e$ are shown for the cases with TM1 and TMS in the same notation as Fig. 9.

Fig. 11. The time profiles of the luminosity of $\bar{\nu}_e$ are shown for the cases with TM1 and TMS in the same notation as Fig. 9.

Figure 1

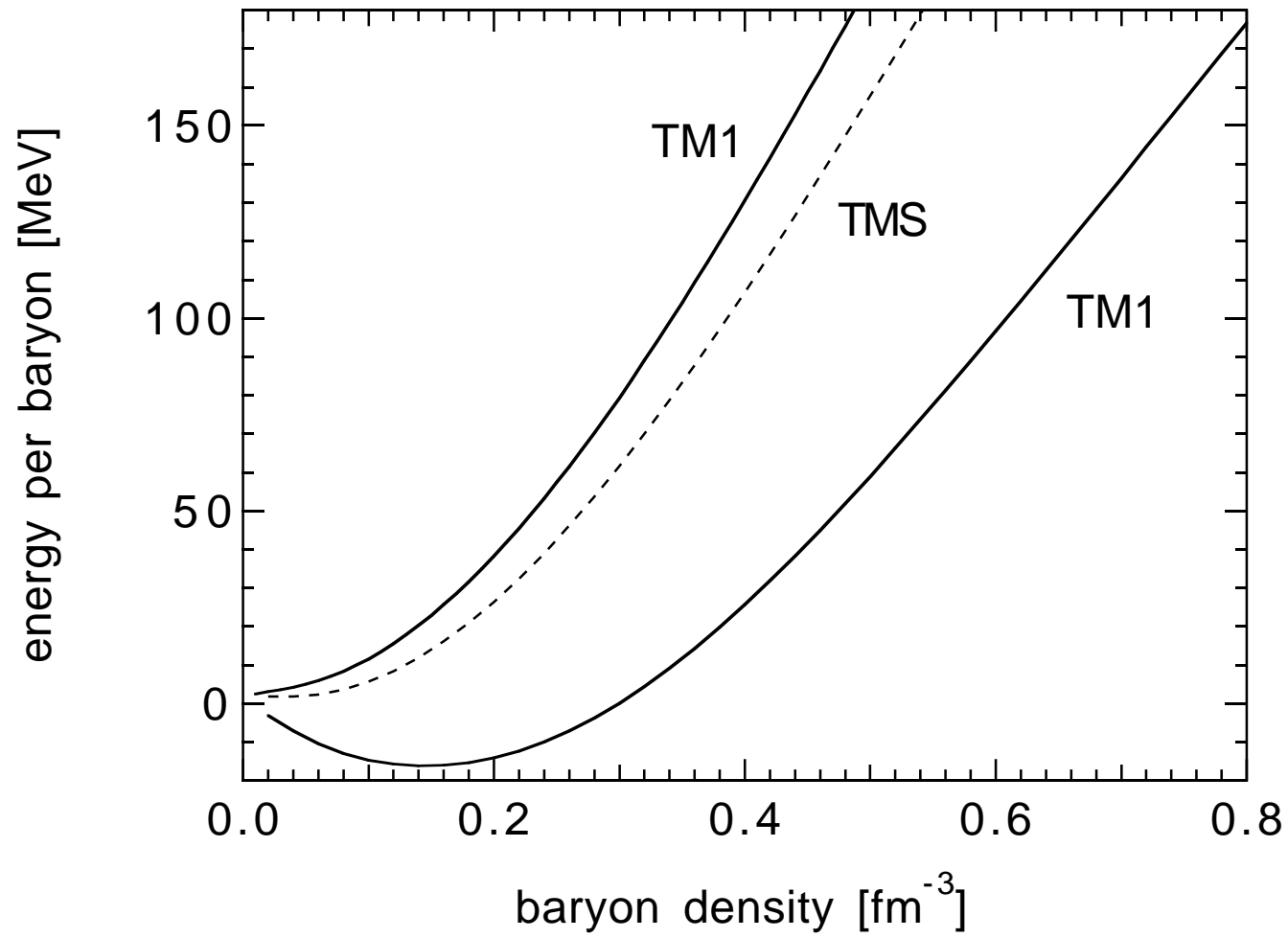


Figure 2-a

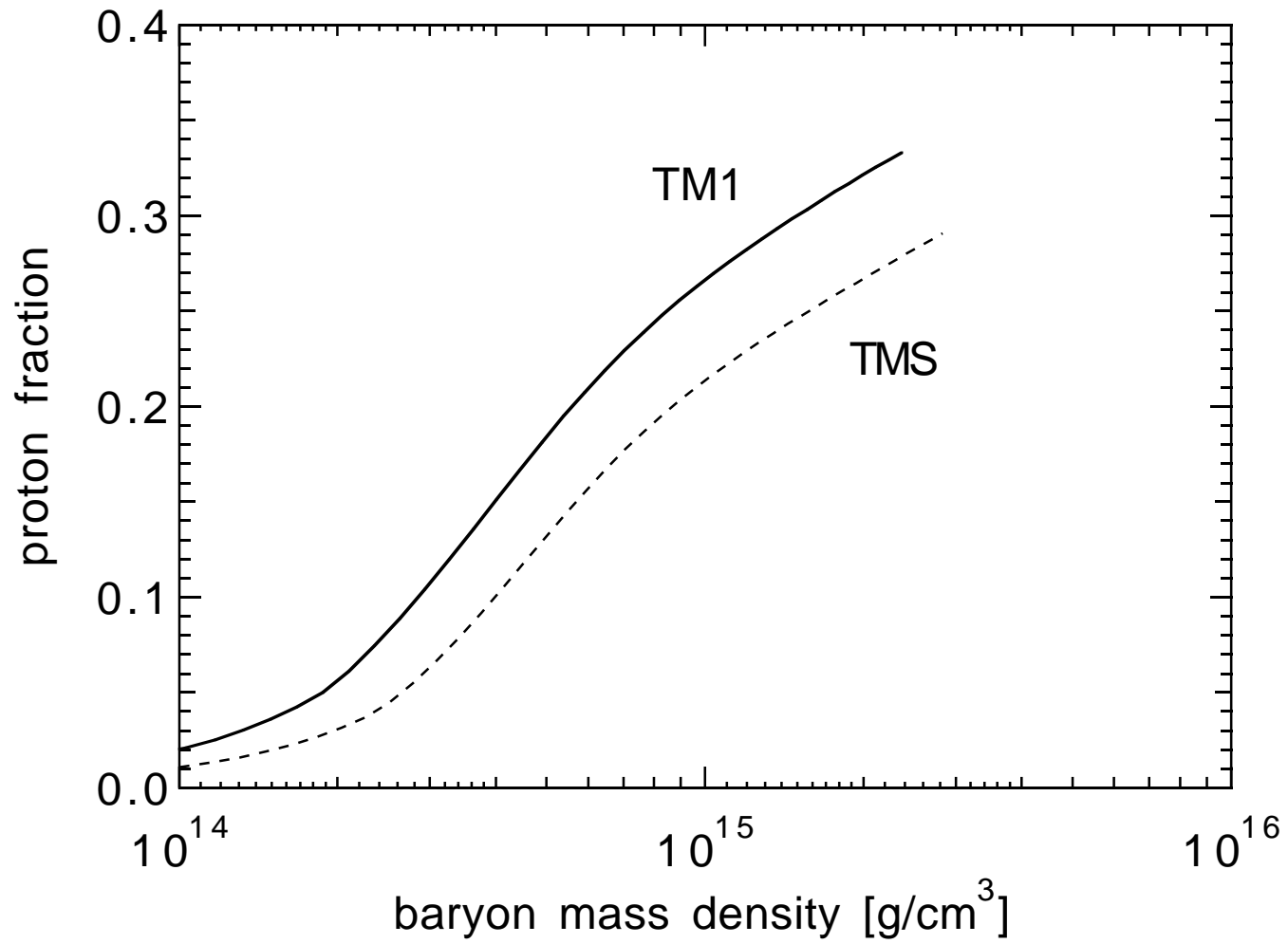


Figure 2-b

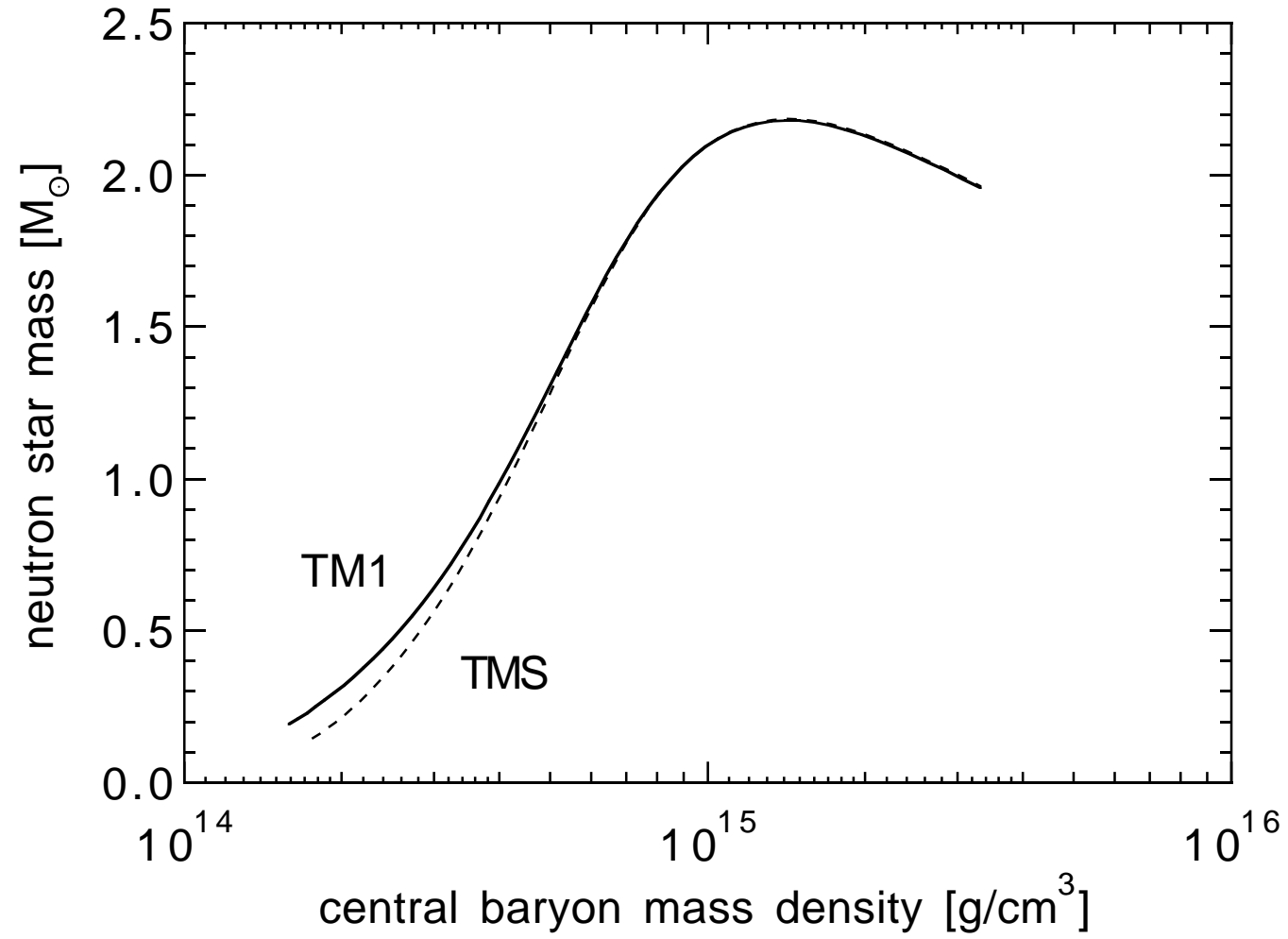


Figure 3

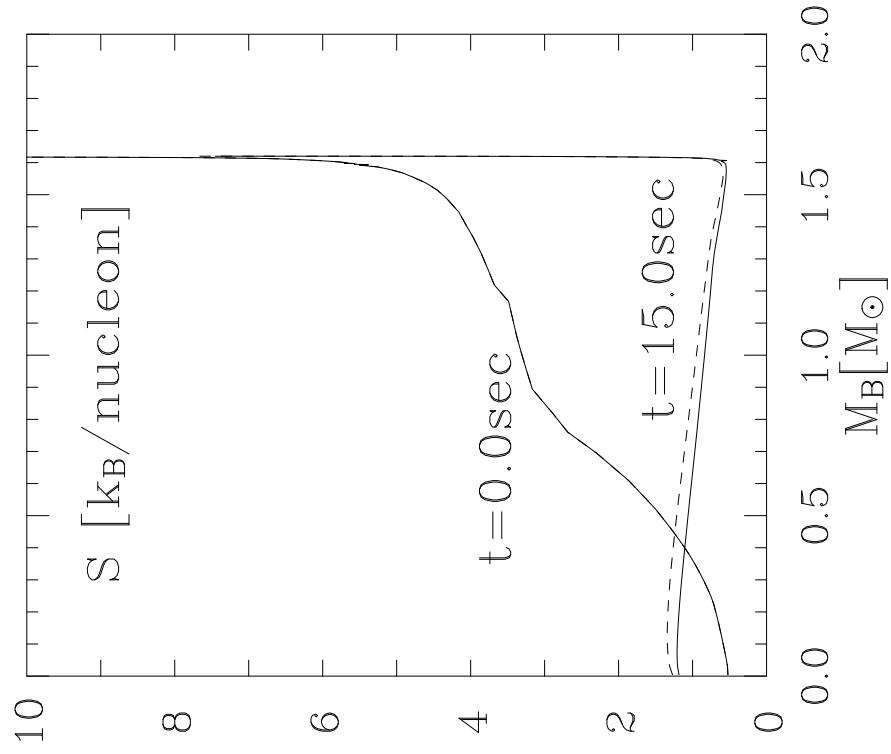


Figure 4

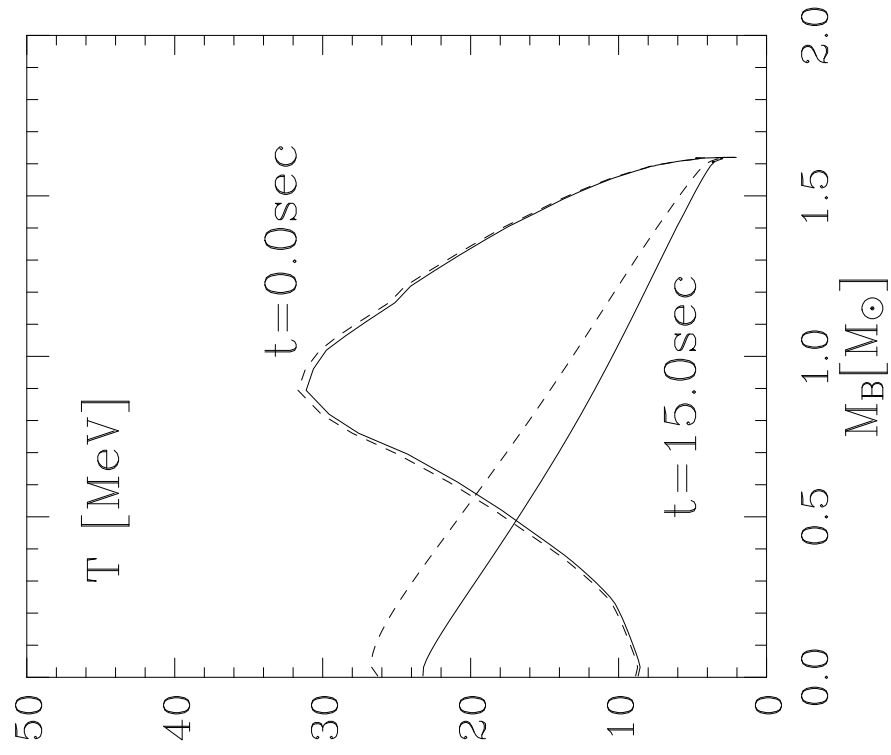


Figure 5

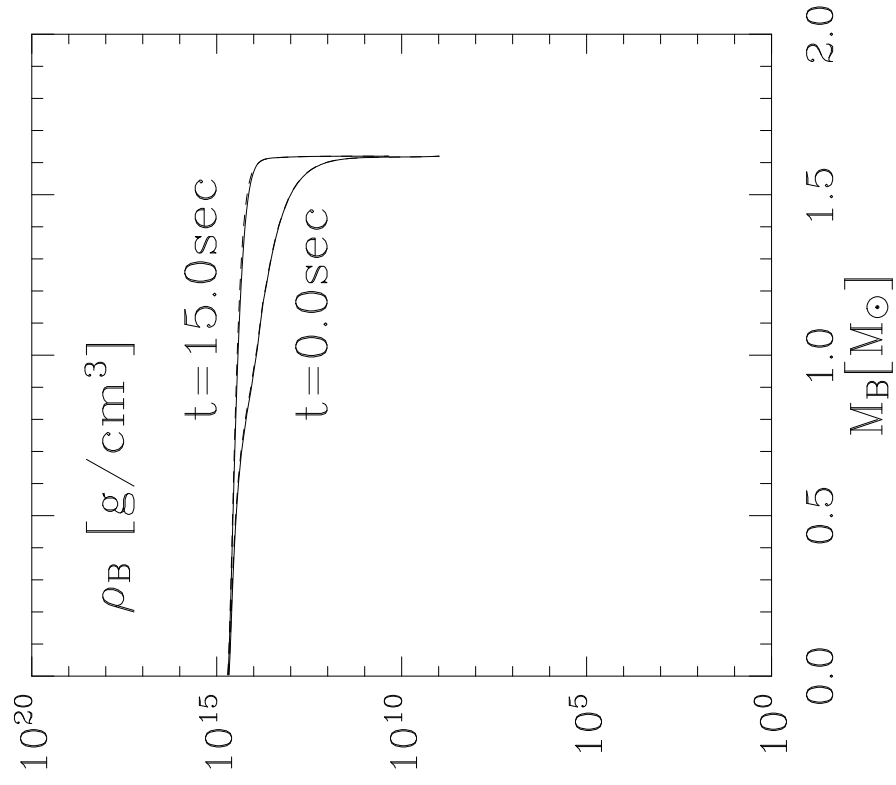


Figure 6

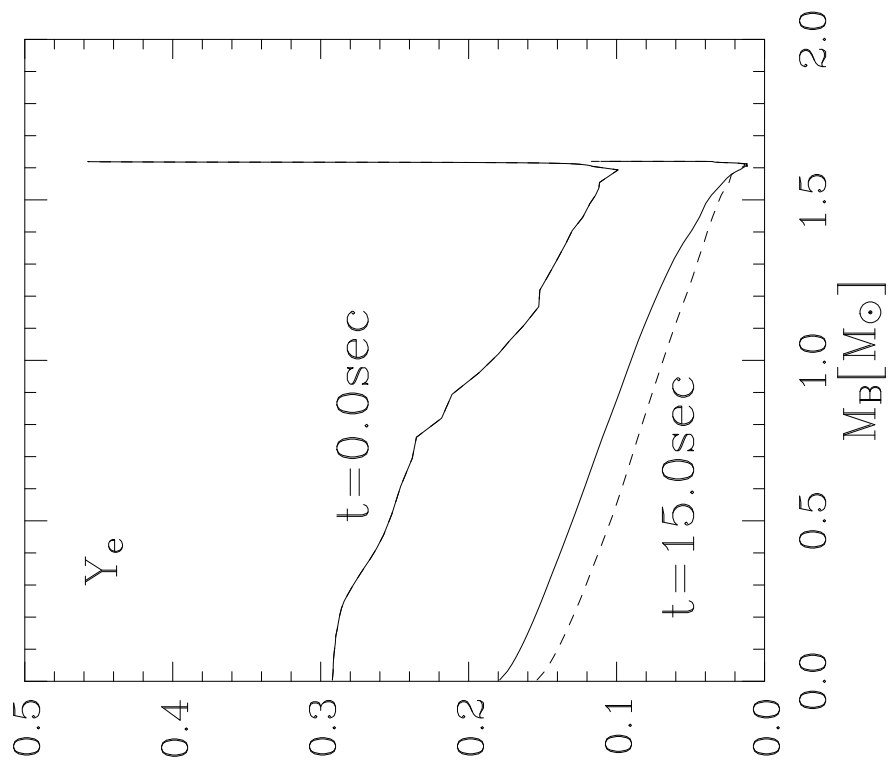


Figure 7

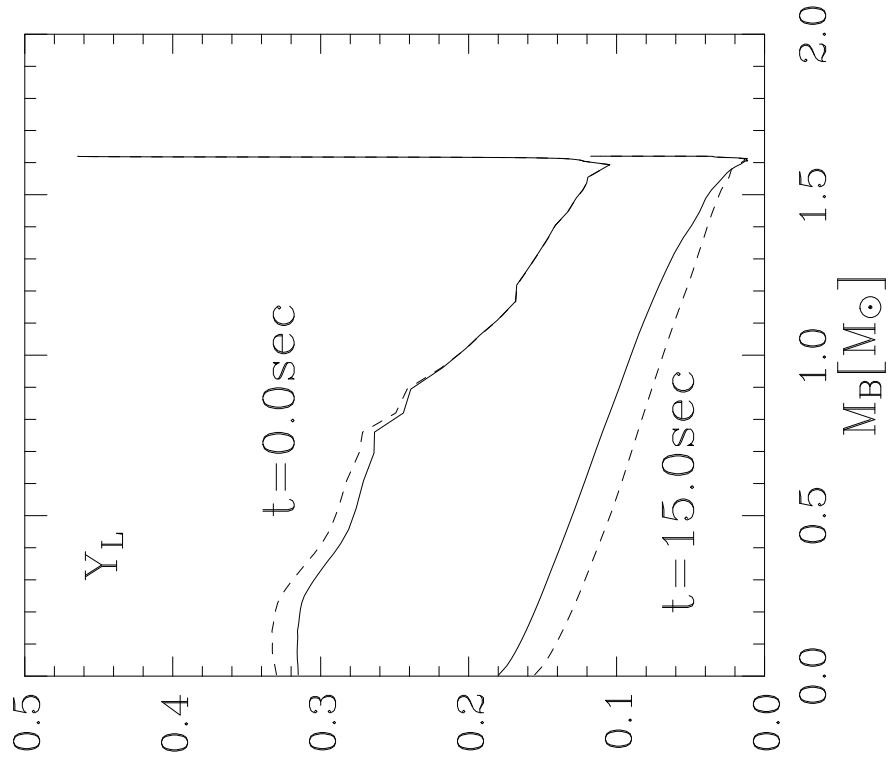


Figure 8

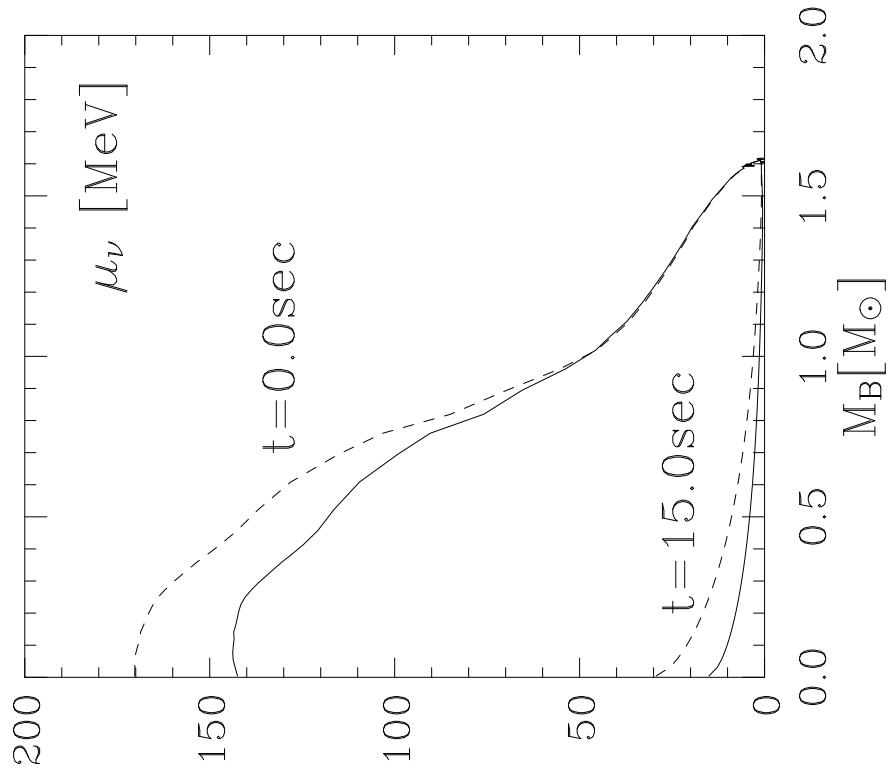


Figure 9

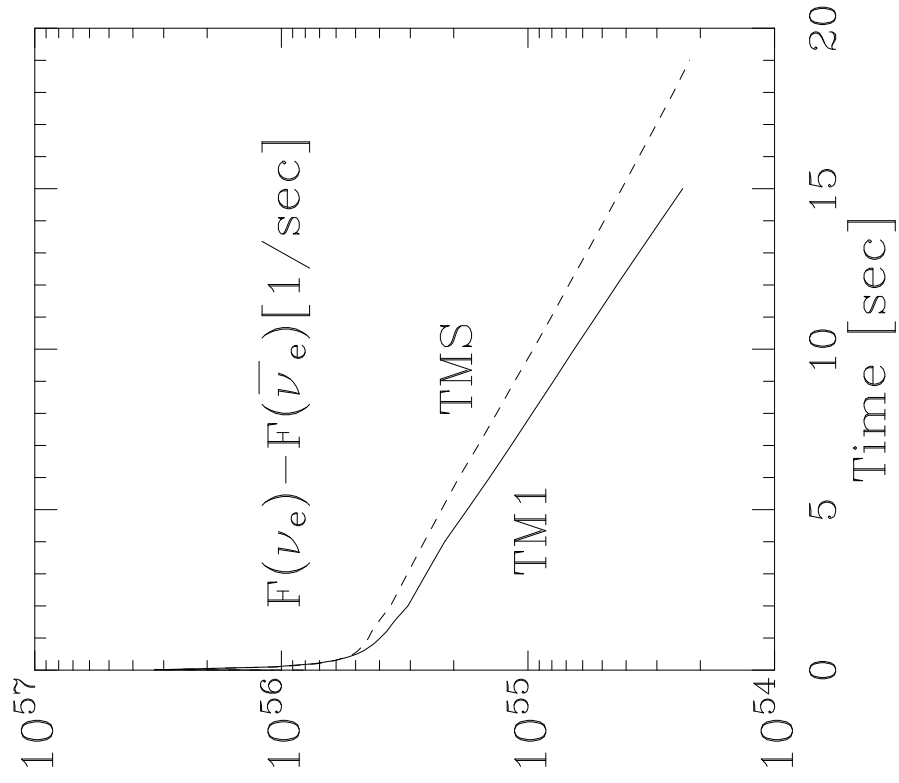


Figure 10

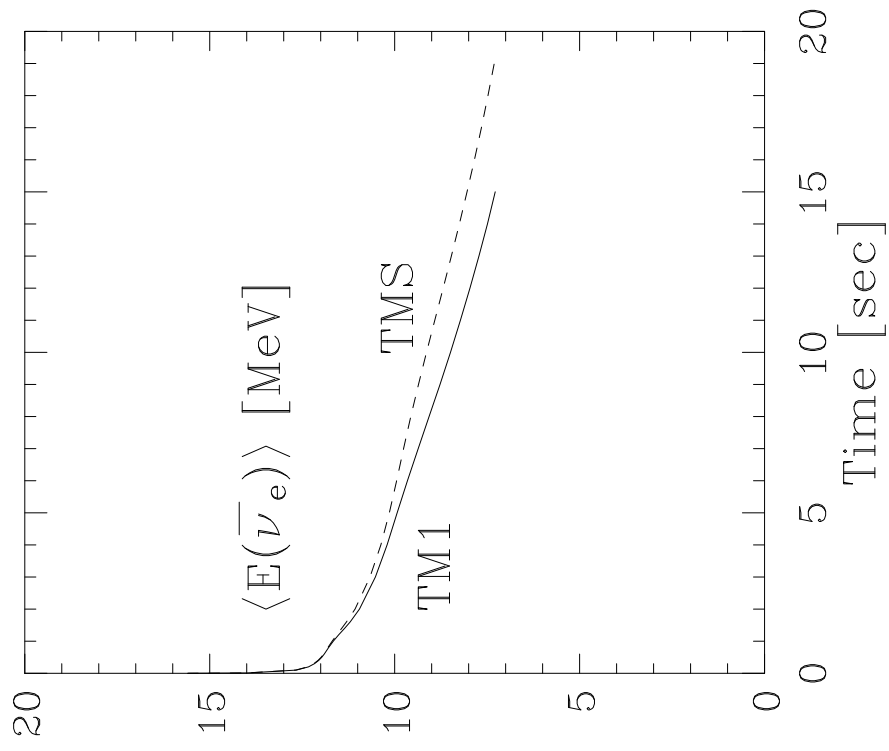


Figure 11

